NANO LETTERS

pubs.acs.org/NanoLett Letter

Origin of Subgap States in Normal-Insulator-Superconductor van der Waals Heterostructures

Paritosh Karnatak,*,▽ Zarina Mingazheva,▽ Kenji Watanabe, Takashi Taniguchi, Helmuth Berger, László Forró, and Christian Schönenberger

Cite This: *Nano Lett.* 2023, 23, 2454−2459 Read Online

ACCESS | Metrics & More | Article Recommendations | Supporting Information

ABSTRACT: Superconductivity in van der Waals materials, such as $NbSe_2$ and TaS_2, is fundamentally novel due to the effects of dimensionality, crystal symmetries, and strong spin−orbit coupling. In this work, we perform tunnel spectroscopy on $NbSe_2$ by utilizing MoS_2 or hexagonal boron nitride (hBN) as a tunnel barrier. We observe subgap excitations and probe their origin by studying various heterostructure designs. We show that the edge of $NbSe_2$ hosts many defect states, which strongly couple to the superconductor and form Andreev bound states. Furthermore, by isolating the $NbSe_2$ edge we show that the subgap states are ubiquitous in MoS_2 tunnel barriers but absent in hBN tunnel barriers, suggesting defects in MoS_2 as their origin. Their magnetic nature reveals a singlet- or a doublet-type ground state, and based on nearly vanishing g factors or avoided crossings of subgap excitations, we highlight the role of strong spin−orbit coupling.

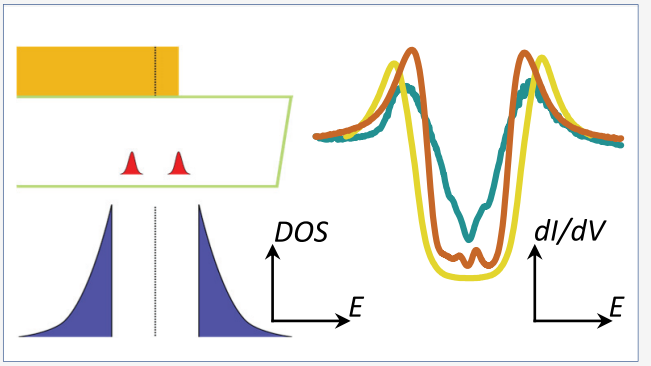

KEYWORDS: *$NbSe_2$, superconductivity, nanostructures, Andreev bound state, subgap excitation, tunneling*

Superconductivity in the two-dimensional limit is driven by a unique interplay among dimensionality, crystal symmetries, correlated electron effects, and, if present, the role of spin−orbit coupling. This often results in various competing ground states and gives rise to rich novel phenomena. Ultimately, two-dimensional van der Waals superconductors are illustrative examples. Naturally superconducting $NbSe_2$ and TaS_2 have been recently isolated and studied,[1,2] and MoS_2 has been doped into a superconducting state.[3] In their monolayer or few-layer forms, these van der Waals superconductors display novel phenomena, such as the survival of superconductivity up to tens of teslas of applied in-plane magnetic field,[1,2] layer -dependent superconducting properties,[2] and competition with other phases.[4] Furthermore, it is predicted that these materials can be externally tuned to host novel topological phases,[5,6] and there are expectations of the presence of unconventional pairing mechanisms in Ising superconductors.[7]

These features essentially result from the large spin−orbit coupling (SOC) and the crystal symmetry in these materials. For this SOC, called the Ising type, the corresponding spin orbit magnetic field points out of plane and in opposite directions in the opposite valleys of the hexagonal Brillouin zone of these materials.[1,3] This splits the spin-degenerate bands, and the majority singlet Cooper pairs are expected to be formed from opposite valleys. As the large spin orbit magnetic field (some estimates indicate $B_{so} \approx 100$ T[3]) pins the spins out of plane, an applied in-plane magnetic field (usually smaller than B_{so}) hardly affects the electron spins and thus the Cooper pairs survive large Zeeman fields.

Recently, proximity-induced superconductivity in semiconducting nanostructures has been widely investigated,[8−12] primarily driven by the proposals for topological quantum computation.[13,14] Additionally, low-dimensional structures coupled to van der Waals superconductors with a large SOC provide a rich platform for investigating the nature of Andreev bound states. They may also offer insights into the unconventional superconducting properties. In this regard, tunnel spectroscopy is a versatile tool for probing the superconducting density of states (DOS). Electronically gapped van der Waals materials provide high-quality tunnel barriers that allow unprecedented control over the barrier thickness and the interface quality. They are also especially well suited to probing the air-sensitive van der Waals superconductors.[15−17] Tunnel spectroscopy in such heterostructures has revealed the presence of Andreev levels in the subgap spectrum.[17,18] However, the exact origin and nature of these bound states

Received: July 13, 2022
Revised: February 21, 2023
Published: March 16, 2023

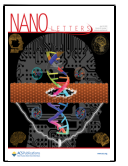

https://doi.org/10.1021/acs.nanolett.2c02777
Nano Lett. 2023, 23, 2454−2459

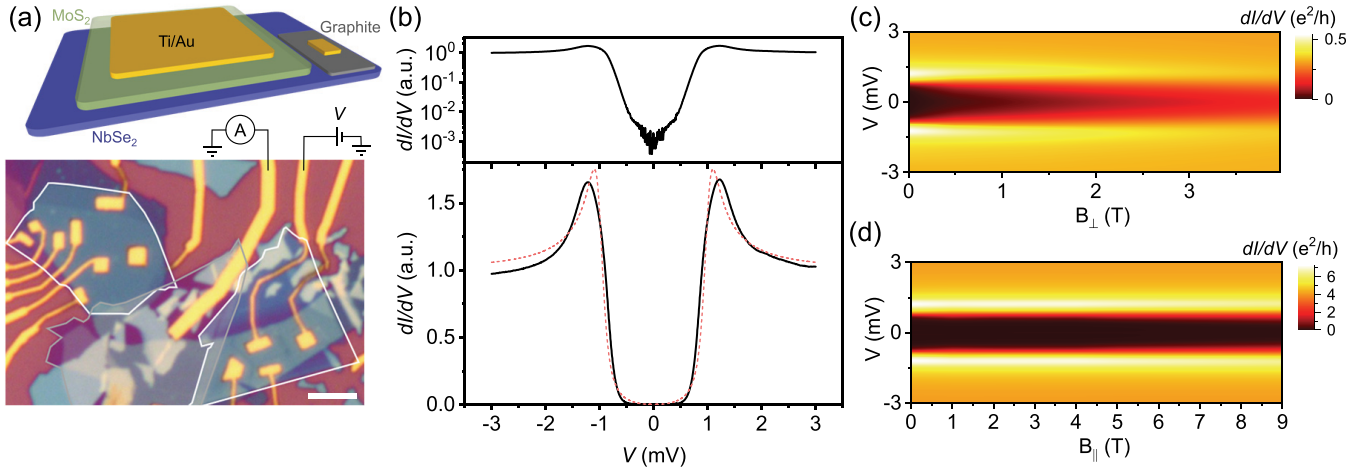

Figure 1. Device design for planar tunneling devices and differential conductance measurements. (a) Schematic shows the normal-insulator-superconductor junctions formed by depositing Ti/Au on the MoS_2 (or hBN) and $NbSe_2$ stack. The optical image shows a typical device with MoS_2 (white outline) and graphite (gray outline) transferred on $NbSe_2$ crystal (bluish color). The scale bar is 5 μm. (b) Measured dI/dV shows a hard superconducting gap with a suppression factor of $G_N/G_0 \approx 800$. The dashed red curve is eq 1 with the parameters $\Delta \approx 1.0$ meV, $\Gamma \approx 0.11$ meV, and $T = 255$ mK. (c) Out-of-plane magnetic field leads to the softening of the superconducting gap. (d) dI/dV measured in an in-plane magnetic field shows that the superconducting gap is robust up to 9 T.

have not been systematically investigated, and it is not known if such bound states reside in the tunnel barriers or are hosted on the $NbSe_2$ surface.[19−21] The role of spin−orbit coupling in determining the Andreev-level ground state and their magnetic nature also remains to be understood.

In this work we perform tunneling spectroscopy on $NbSe_2$ by utilizing MoS_2 or hexagonal boron nitride (hBN)[22] as a tunnel barrier and Ti/Au as the normal leads. We find that the single-particle gapped spectrum is often interrupted by the presence of subgap excitations, and we probe their origin by studying various heterostructure designs. We show that the edge of $NbSe_2$ hosts many defect states, some of which are strongly coupled to the superconductor. However, we also observe subgap excitations in devices where the $NbSe_2$ edge is electrically isolated. We show that these subgap excitations arise from defects in MoS_2 and are absent in hBN tunnel barriers. We probe the magnetic nature of these subgap states by studying their evolution in applied magnetic fields and reveal the nature of ground states as well as highlight the role of spin−orbit coupling.

The normal-insulator-superconductor (NIS)-type planar tunnel junctions are fabricated by stacking MoS_2 (three to five layers) or hBN (three layers) on $NbSe_2$ crystals (∼3−20 nm) in a glovebox in an N_2 atmosphere. MoS_2 or hBN acts as the tunnel barrier and prevents $NbSe_2$ from oxidation; see the schematic and a representative device image in Figure 1a. We have studied 8 devices and more than 50 tunnel junctions, and a summary of results is presented here. Further details of fabrication, device parameters, and measurements can be found in the Supporting Information (SI).

The differential conductance across an NIS junction can be written as[23,24]

$$\frac{dI}{dV} \propto \int_{-\infty}^{+\infty} N_S(E, \Gamma, \Delta) \frac{df(E - eV, T)}{dV} dE \quad (1)$$

where N_S is the single-particle DOS as a function of energy E for the superconducting electrode with a superconducting gap Δ and a broadening parameter Γ; $f(E, T)$ is the Fermi−Dirac distribution at a finite temperature T; and V is the bias voltage applied across the tunnel barrier. The superconducting DOS can be modeled by the Dynes formula[25]

$$N_S(E, \Gamma, \Delta) = Re\left\{\frac{E - i\Gamma}{\sqrt{(E - i\Gamma)^2 - \Delta^2}}\right\} \quad (2)$$

It is instructive to see that at zero temperature eq 1 reduces to $dI/dV \propto N_S(eV, \Gamma, \Delta)$ and the differential conductance measurement across a tunnel barrier probes the DOS of the superconductor. At finite temperature, the DOS features are broadened by $\sim k_B T$. One such measurement is shown in Figure 1b, with a well-defined superconducting gap and a suppression factor $G_N/G_0 \gtrsim 800$, where G_0 and G_N are the differential conductance in the superconducting gap (typically at $V = 0$ or the minimum conductance in the gap) and outside the gap (typically $V \approx 3$ mV), respectively, as emphasized on the log scale in the top panel of Figure 1b. We typically observe hard gaps across our tunnel barriers with $G_N/G_0 \gtrsim 100$, indicating high-quality tunnel barriers and consequently the suppression of Andreev processes. A plot of eq 1 with a gap of $\Delta \approx 1.0$ meV and broadening parameter $\Gamma \approx 0.11$ meV is shown in Figure 1b. (See the Supporting Information for further discussion on gap fitting.) Moreover, dI/dV measurements performed in a perpendicular magnetic field reveal significant softening of the superconducting gap (Figure 1c), as expected for $NbSe_2$ at this scale due to the orbital depairing.[26,27] However, the Ising protection against an applied in-plane magnetic field is noticeable for $NbSe_2$, as seen in Figure 1d. We observe that the superconducting gap is robust ($G_N/G_0 \approx 100$) up to 9 T, limited only by the cryostat magnet. This allows us to study the behavior of the subgap states in a large (in-plane) magnetic field, as discussed later.

Unlike the spectrum shown in Figure 1b, however, we often observe discrete subgap features in MoS_2 tunnel barrier junctions (Figure 2a). Such subgap features can result from discrete electronic states in the tunnel path, modified by the superconducting proximity effect. The discrete states themselves may arise from a defect or an impurity in the tunnel barrier or on the surface of the superconductor.[19−21] The

https://doi.org/10.1021/acs.nanolett.2c02777
Nano Lett. 2023, 23, 2454−2459

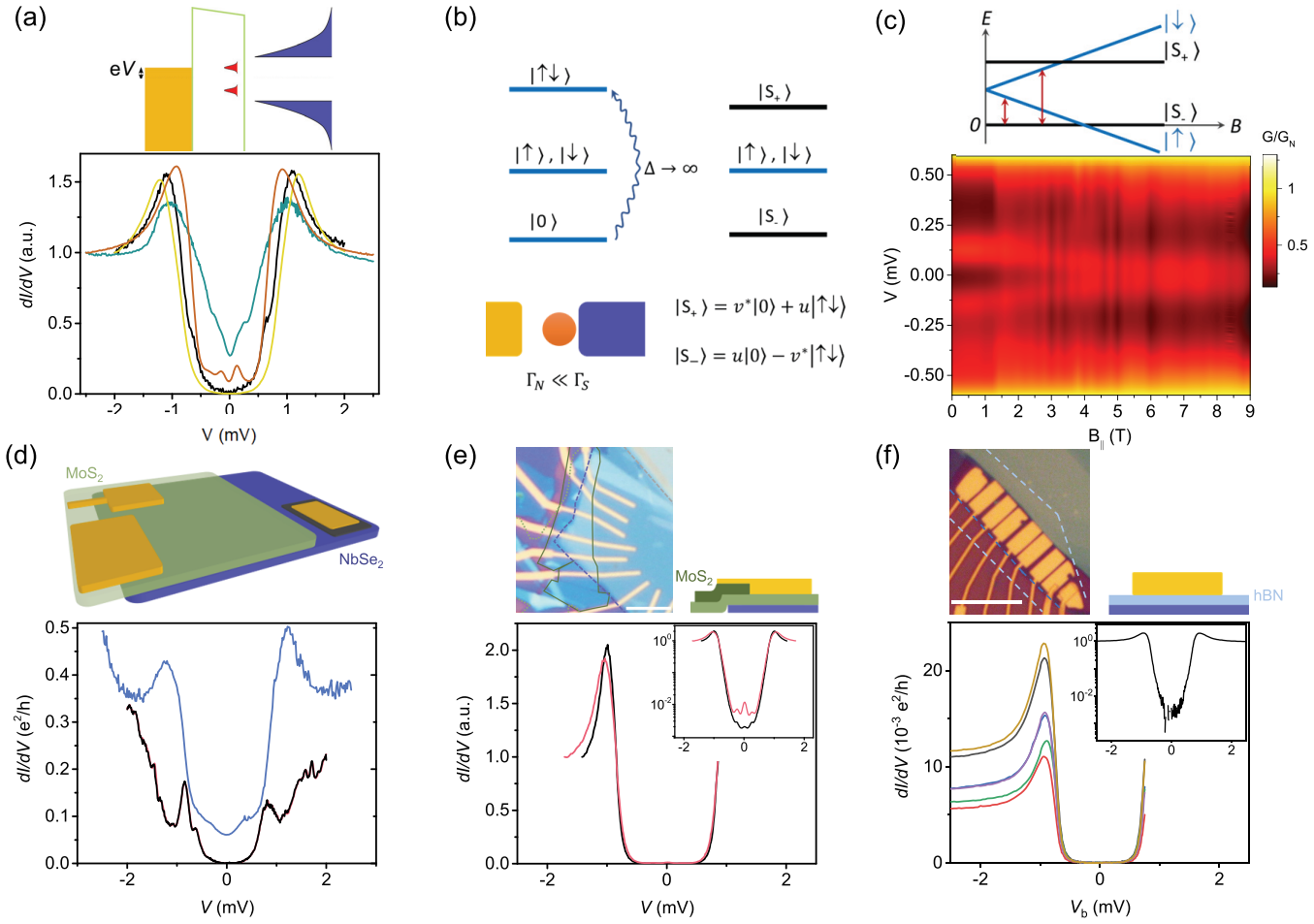

Figure 2. Origin of subgap states. (a) dI/dV measurements show the presence of subgap excitations. Schematic shows a possible mechanism where a defect strongly couples to the superconductor. Normalized dI/dV is shown for four different junctions in device D10. (b) Electronic states in a quantum dot are modified when it is strongly coupled to the superconductor. (c) Magnetic field evolution of the subgap excitations indicates that at $B = 0$ the ground state is a singlet but the system undergoes a quantum phase transition to a doublet ground state at a finite magnetic field. Red arrows denote the excitation energies in the schematic. The jumps in magnetic field are a result of the imperfect alignment of $B_{\|}$ that leads to discrete units of flux entering the tunnel junction area. (d) dI/dV measurements on the edge of $NbSe_2$. Repeated runs are shown by black and red lines (barely visible, lie on top of each other), while another edge contact is shown in blue. (e) dI/dV measurements with the edge of $NbSe_2$ electrically isolated by using a thicker MoS_2 (solid green outline) at the edge of $NbSe_2$ (blue dashed line). Scale bar is 5 μm. The inset on a log scale highlights the presence of subgap excitations. (f) dI/dV measurements for hBN used as a tunnel barrier show the absence of subgap excitations. The inset on a log scale shows the absence of subgap excitation down to the measurement noise floor. The scale bar in the optical image is 10 μm.

formation of such Andreev levels has recently been widely explored, especially in semiconducting nanowires coupled to superconductors, and is fairly well understood.[9,11,12] We model the defect state as a quantum dot coupled to a superconductor. A spin-degenerate single orbital level in an isolated quantum dot has four eigenstates $|0\rangle$, $|\uparrow\rangle$, $|\downarrow\rangle$, and $|\uparrow\downarrow\rangle$. When the quantum dot couples to a superconductor, the empty $|0\rangle$ and the doubly occupied states $|\uparrow\downarrow\rangle$ are hybridized via virtual Andreev processes that exchange two electrons with the dot, as shown in the schematic in Figure 2b. If the quasiparticles in the superconductor can be neglected ($\Delta \to \infty$, the so-called superconducting atomic limit), then this hybridization results in two BCS-like singlet eigenstates $|S_-\rangle = u|0\rangle - v^*|\uparrow\downarrow\rangle$ and $|S_+\rangle = v|0\rangle + u^*|\uparrow\downarrow\rangle$, given by the Bogoliubov−de Gennes (BdG) transformation,[28−30] where u and v are the BdG amplitudes. For single average occupancy of the dot, the system has two possible ground states: either the degenerate doublet $|\uparrow\rangle$, $|\downarrow\rangle$ or the singlet eigenstate $|S_-\rangle$. The energy of the singlet states is given by[29]

$$E_{\pm} = U/2 \pm \sqrt{\xi_d^2 + \Gamma_s^2} + \xi_d$$

where U is the charging energy, $\xi_d = \epsilon_d + U/2$ with ϵ_d being the bare energy of the doublet states $\{|\uparrow\rangle, |\downarrow\rangle\}$, and Γ_s is the coupling to the superconductor. Therefore, the competition between the ground states $\{|\uparrow\rangle, |\downarrow\rangle\}$ and $|S_-\rangle$ depends on the relative magnitudes of various energy scales in the system. In general, a stronger coupling Γ_s to the superconductor favors a singlet $|S_-\rangle$ ground state whereas a large charging energy U results in a doublet ground state $\{|\uparrow\rangle, |\downarrow\rangle\}$. In this work, we discuss the subgap features in terms of the Andreev bound states, and this framework holds when the quasiparticles in the superconductor do not play a role. However, in principle our experiments cannot distinguish if the singlet is the superposition of $|0\rangle$ and $|\uparrow\downarrow\rangle$ (Andreev bound state) or is formed between one electron on the dot and another on the superconductor (Yu−Shiba−Rushinov state).[31−33] Quasiparticles in the superconductor could play a role if $\Delta \approx \Gamma_s$.

https://doi.org/10.1021/acs.nanolett.2c02777
Nano Lett. 2023, 23, 2454−2459

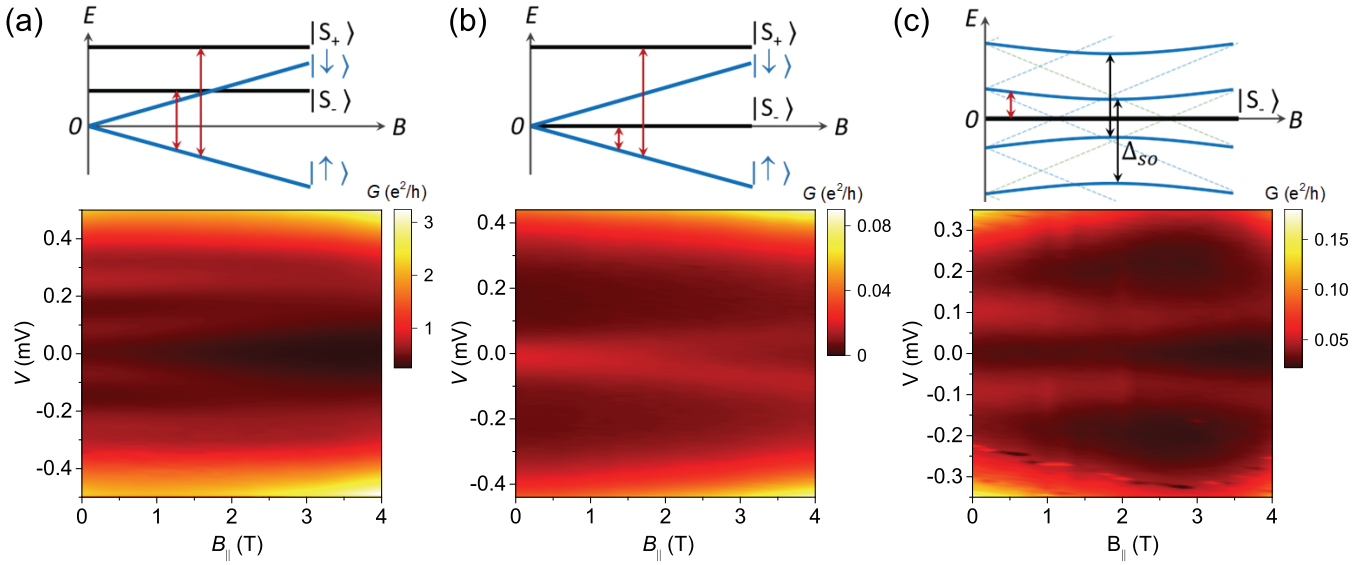

Figure 3. Anomalous subgap excitations. (a) Multiple subgap states are seen at $B = 0$. They evolve with an applied in-plane magnetic field but with a different g factor. (b) dI/dV measurements show a zero bias excitation at $B = 0$, which splits in the magnetic field. The transition to the higher singlet is likely at the gap edge and is not visible in our measurement. (c) Subgap excitations show an avoided crossing feature with a minimal splitting of ∼0.185 meV at $B_\parallel \approx 2$ T.

Applying a dc voltage bias V across the tunnel barrier, which is equivalent to the energy of the excited state, results in the transfer of a single electron into the dot (with N electrons) from the normal lead. This electron can form a Cooper pair to enter the superconductor; consequently, a hole is retro-reflected into the normal lead. Symmetric across the Fermi energy, a time-reversed process occurs and can be observed as a similar feature at the opposite dc voltage bias. Thus, the electron−hole symmetric subgap features in tunnel spectroscopy probe the excitation energy of the subgap states (N to $N \pm 1$ transitions) in the lowest order. An external magnetic field causes Zeeman splitting of the spin-degenerate doublet states and provides a key tool to study the nature of the localized ground states. See Figure 2c and the discussion later.

We first investigate the origin of such subgap excitations: whether they reside in the tunnel barrier or on the surface of the superconductor.[19−21] We notice that the tunnel junctions with a large overlap with the edge of the $NbSe_2$ crystal exhibit multiple features in dI/dV both outside and inside the gap (Figure 2d). The repeatability of these features in multiple sweeps indicates that they represent discrete energy levels and do not arise from time-dependent noise. They likely arise from defects present at the $NbSe_2$ edge cleaved during exfoliation, some of which strongly couple to the superconductor and show up as subgap excitations. The features outside the gap may be understood as resonant features arising in the normal-dot-normal system. While it may not be surprising that the $NbSe_2$ edge hosts many defects, this may be critical for the topological edge states predicted in $NbSe_2$ with an applied in-plane magnetic field.[5,6] Instead, it would be crucial to engineer the boundary of the topological and the trivial phase on the bulk of $NbSe_2$, as in a recent study.[34]

In a simple planar tunnel junction, a part of the normal "wire" always crosses the $NbSe_2$ edge (Figure 2d schematic). Therefore, next we address whether all of the subgap states that we observe arise from such defect states at the edge of $NbSe_2$. We do this by electrically isolating the $NbSe_2$ edge by transferring additional MoS_2 layers over the edge of $NbSe_2$; see the optical image and the schematic in Figure 2e. The corresponding dI/dV curves plotted in Figure 2e exhibit a well-behaved superconducting gap. The subgap states are now rare but still present in multiple junctions, as shown in the inset. This points to other sources of defect states, in addition to those at the edge of the $NbSe_2$ crystal. The possibilities that remain are the defect states in the tunnel barrier or on the surface of the superconductor.

To address this, we replace the MoS_2 tunnel barrier with three layers of hBN, known to be an effective tunnel barrier. In particular, the defect density in hBN is small[22,35] and likely 3 orders of magnitude smaller than that in MoS_2,[36−39] although we are not aware of direct comparative studies. The differential conductance for six such tunnel junctions, each with an area of ∼10 μm^2, is shown in Figure 2f. While tunnel spectroscopy shows a well-behaved superconducting gap with a suppression factor of $G_N/G_0 \approx 300$, we do not observe subgap features in any hBN tunnel junction down to our measurement resolution, as evident from the log-scale plot in the inset of Figure 2f. This leads us to believe that the subgap features in $MoS_2/NbSe_2$ tunnel junctions arise either from the edge of the $NbSe_2$ crystal or from defects in MoS_2 that strongly couple to the superconductor.

Furthermore, we study the subgap excitation spectrum in an applied in-plane magnetic field. The Zeeman splitting of the doublet states $\{|\uparrow\rangle, |\downarrow\rangle\}$ results in unique features in the excitation spectrum which allows the identification of the ground state. One such measurement is shown in Figure 2c, where at $B_\parallel = 0$ two subgap excitations are visible at $V \approx \pm 0.13$ mV. With an applied in-plane magnetic field $B_\parallel$, the subgap features split (effective g factor of ∼0.7), where one branch moves toward zero bias and the other (weakly visible for $V > 0$) moves toward the gap edge. (See the SI for the second derivative.) The overall behavior can be understood by considering that the dot is in a singlet $|S_-\rangle$ ground state at $B_\parallel = 0$. At $V \approx 0.13$ mV, the chemical potential of the normal lead is aligned to the spin-degenerate doublet excited state. With increasing $B_\parallel$, the doublet splits, resulting in the

https://doi.org/10.1021/acs.nanolett.2c02777
Nano Lett. 2023, 23, 2454−2459

excitation energy to the lower branch decreasing while the excitation energy to the upper branch increases, as illustrated in the Figure 2c schematic. In fact, for increasing $B_{\|}$ when the lower branch crosses zero energy, the system undergoes a quantum phase transition and the ground state changes to the doublet ground state. See the SI for an example. The appearance of the bound state sticking to zero energy for $B_{\|} > 6$ T is either the result of two wide (fwhm $\approx$ 0.18 meV) bound states crossing or the influence of spin−orbit mixing with higher orbital levels, as discussed later.

The ground state of the dot coupled to a superconductor depends on the relative strengths of various energy scales: the tunnel coupling of the dot to the superconductor Γ_s, the charging energy U, the superconducting gap Δ, and the energy of the dot level relative to the chemical potential of the superconductor ξ_d. Since a finite Γ_s is necessary for the visibility of the subgap excitations and a large Γ_s favors a singlet ground state, we observe singlet states nearly 6 times as frequently as doublet ground states. (See the SI for a count of ground states.) One such case is shown in Figure 3a, where the excitations at $\sim\pm$0.08 meV ($B_{\|} = 0$) move to higher absolute energies with an applied $B_{\|}$, as expected for a doublet ground state. The schematic in Figure 3a demonstrates the mechanism. The subgap excitation visible at higher energies of $\sim\pm$0.25 meV ($B_{\|} = 0$) may be attributed to the transition to the higher singlet, but this is unlikely due to a different g factor. Instead, this may result from another parallel Andreev bound state formed via a second defect, in a junction of size $\sim$3.5 μm^2, and a large SOC may result in a nearly vanishing g factor as discussed later.

For some junctions, a zero-bias peak is also observed at $B_{\|} = 0$ which splits for finite $B_{\|}$, as shown in Figure 3b. We believe this results from an accidental degeneracy of the doublet and the lower singlet $|S_-\rangle$, as shown in the Figure 3b schematic. Such a spectrum could also result from a doublet ground state where inelastic co-tunneling transitions occur between the two states of the spinful doublet. However, we believe that the transfer of charge through the parity-conserving doublet is strongly suppressed due to (a) the hard gap that we observe and (b) the consequently fourth-order nature of this process. We therefore think that we do not observe them in any of our experiments.

Finally, an avoided-crossing-like feature is shown in Figure 3c, where the subgap excitations move toward zero bias but at $B_{\|} \approx 2$ T they start to move to higher absolute energies. We attribute this to the spin mixing and hybridization of the doublet states that arise from higher orbital levels, due to SOC in the host material,[40] as illustrated in the Figure 3c schematic. The size of the splitting depends on the details of the defect which determine the strength of SOC and the relative directions of B_{SO} and $B_{\|}$. No hybridization occurs when the externally applied magnetic field is parallel to the internal spin orbit field.[41,42] This may explain why splitting is not observed in other junctions. A large spin−orbit gap (compared to the doublet excitation energy) would also result in a reduced effective g factor (see also Figure 3a).

In conclusion, we have performed tunnel spectroscopy on $NbSe_2$ by utilizing MoS_2 or hexagonal boron nitride (hBN) as a tunnel barrier and Ti/Au as the normal leads. We find that the single-particle gapped spectrum often exhibits the presence of subgap excitations, and we probe their origin by studying various heterostructure designs. We show that the edge of $NbSe_2$ hosts many defect states, some of which are strongly coupled to the superconductor. However, we also observe subgap excitations in devices where the $NbSe_2$ edge is electrically isolated. We show that while the subgap excitations are fairly ubiquitous in MoS_2 tunnel barriers they are absent in hBN tunnel barriers, suggesting that these subgap excitations arise from the defects in MoS_2. The evolution of subgap excitations in an applied in-plane magnetic field allows us to probe the magnetic nature of the participating subgap states and reveals the nature of subgap ground states. Subgap excitations that anticross or show no dispersion with the Zeeman field highlight the role of spin−orbit coupling in the system.

■ ASSOCIATED CONTENT

Data Availability Statement

All data in this publication are available in numerical form at https://doi.org/10.5281/zenodo.6817129.

Supporting Information

The Supporting Information is available free of charge at https://pubs.acs.org/doi/10.1021/acs.nanolett.2c02777.

Detailed descriptions of device fabrication, experimental methods, and complementary measurements (PDF)

■ AUTHOR INFORMATION

Corresponding Author

Paritosh Karnatak − *Department of Physics, University of Basel, CH-4056 Basel, Switzerland;* orcid.org/0000-0001-8233-0887; Email: paritosh.karnatak@unibas.ch

Authors

Zarina Mingazheva − *Department of Physics, University of Basel, CH-4056 Basel, Switzerland*

Kenji Watanabe − *Research Center for Functional Materials, National Institute for Material Science, Tsukuba 305-0044, Japan;* orcid.org/0000-0003-3701-8119

Takashi Taniguchi − *International Center for Materials Nanoarchitectonics, National Institute for Materials Science, Tsukuba 305-0044, Japan;* orcid.org/0000-0002-1467-3105

Helmuth Berger − *Institute of Condensed Matter Physics, Ecole Polytechnique Fédérale de Lausanne, CH-1015 Lausanne, Switzerland*

László Forró − *Institute of Condensed Matter Physics, Ecole Polytechnique Fédérale de Lausanne, CH-1015 Lausanne, Switzerland; Stavropoulos Center for Complex Quantum Matter, Department of Physics, University of Notre Dame, Notre Dame, Indiana 46556, United States*

Christian Schönenberger − *Department of Physics and Swiss Nanoscience Institute, University of Basel, CH-4056 Basel, Switzerland;* orcid.org/0000-0002-5652-460X

Complete contact information is available at: https://pubs.acs.org/10.1021/acs.nanolett.2c02777

Author Contributions

P.K. and C.S. designed the experiments. P.K. and Z.M. fabricated the devices and performed the measurements. With input from C.S., P.K. and Z.M. performed the data analysis. H.B. and L.F. provided $NbSe_2$ crystals. K.W. and T.T. provided hBN crystals. P.K. and Z.M. wrote the manuscript, with input from all authors.

Author Contributions

$^{\nabla}$P.K. and Z.M. made equal contributions.

Notes

The authors declare no competing financial interest.

■ ACKNOWLEDGMENTS

We thank Hadar Steinberg, Andreas Baumgartner, and Jelena Klinovaja for fruitful discussions. This project has received funding from the European Research Council (ERC) under the European Union's Horizon 2020 research and innovation programme (grant agreement no. 787414 TopSupra) by the Swiss National Science Foundation through the National Centre of Competence in Research Quantum Science and Technology (QSIT) and by the Swiss Nanoscience Institute (SNI). K.W. and T.T. acknowledge support from the Elemental Strategy Initiative conducted by MEXT, Japan and the CREST (JPMJCR15F3), JST and from JSPS KAKENHI (grant nos. 19H05790 and 20H00354).

■ REFERENCES

(1) Xi, X.; et al. Ising pairing in superconducting $NbSe_2$ atomic layers. *Nat. Phys.* **2016**, *12*, 139−143.
(2) de la Barrera, S. C.; Sinko, M. R.; Gopalan, D. P.; Sivadas, N.; Seyler, K. L.; Watanabe, K.; Taniguchi, T.; Tsen, A. W.; Xu, X.; Xiao, D.; Hunt, B. M.; et al. Tuning ising superconductivity with layer and spin−orbit coupling in two-dimensional transition-metal dichalcogenides. *Nat. Commun.* **2018**, *9*, 1427.
(3) Lu, J.; et al. Evidence for two-dimensional ising superconductivity in gated MoS_2. *Science* **2015**, *350*, 1353−1357.
(4) Yang, Y.; et al. Enhanced superconductivity upon weakening of charge density wave transport in 2H-TaS_2 in the two-dimensional limit. *Phys. Rev. B* **2018**, *98*, 035203.
(5) He, W.-Y.; et al. Magnetic field driven nodal topological superconductivity in monolayer transition metal dichalcogenides. *Communications Physics* **2018**, *1*, 40.
(6) Shaffer, D.; Kang, J.; Burnell, F. J.; Fernandes, R. M. Crystalline nodal topological superconductivity and bogolyubov fermi surfaces in monolayer $NbSe_2$. *Phys. Rev. B* **2020**, *101*, 224503.
(7) Möckli, D.; Khodas, M. Robust parity-mixed superconductivity in disordered monolayer transition metal dichalcogenides. *Phys. Rev. B* **2018**, *98*, 144518.
(8) Schindele, J.; Baumgartner, A.; Schönenberger, C. Near-unity cooper pair splitting efficiency. *Physical review letters* **2012**, *109*, 157002.
(9) Schindele, J.; Baumgartner, A.; Maurand, R.; Weiss, M.; Schönenberger, C. Nonlocal spectroscopy of andreev bound states. *Phys. Rev. B* **2014**, *89*, 045422.
(10) Buitelaar, M.; Nussbaumer, T.; Schönenberger, C. Quantum dot in the kondo regime coupled to superconductors. *Phys. Rev. Lett.* **2002**, *89*, 256801.
(11) De Franceschi, S.; Kouwenhoven, L.; Schönenberger, C.; Wernsdorfer, W. Hybrid superconductor−quantum dot devices. *Nature Nanotechnol.* **2010**, *5*, 703−711.
(12) Lee, E. J.; et al. Spin-resolved andreev levels and parity crossings in hybrid superconductor−semiconductor nanostructures. *Nature Nanotechnol.* **2014**, *9*, 79−84.
(13) Lutchyn, R. M.; Sau, J. D.; Sarma, S. D. Majorana fermions and a topological phase transition in semiconductor-superconductor heterostructures. *Physical Review Letters* **2010**, *105*, 077001.
(14) Oreg, Y.; Refael, G.; Von Oppen, F. Helical liquids and majorana bound states in quantum wires. *Physical review letters* **2010**, *105*, 177002.
(15) Khestanova, E.; et al. Unusual suppression of the superconducting energy gap and critical temperature in atomically thin $NbSe_2$. *Nano Lett.* **2018**, *18*, 2623−2629.
(16) Dvir, T.; et al. Spectroscopy of bulk and few-layer superconducting $NbSe_2$ with van der waals tunnel junctions. *Nat. Commun.* **2018**, *9*, 598.
(17) Dvir, T.; Aprili, M.; Quay, C. H. L.; Steinberg, H. Zeeman tunability of andreev bound states in van der waals tunnel barriers. *Phys. Rev. Lett.* **2019**, *123*, 217003.
(18) Devidas, T.; Keren, I.; Steinberg, H. Spectroscopy of $NbSe_2$ using energy-tunable defect-embedded quantum dots. *Nano Lett.* **2021**, *21*, 6931−6937.
(19) Ménard, G. C.; et al. Coherent long-range magnetic bound states in a superconductor. *Nat. Phys.* **2015**, *11*, 1013−1016.
(20) Kezilebieke, S.; Dvorak, M.; Ojanen, T.; Liljeroth, P. Coupled yu−shiba−rusinov states in molecular dimers on $NbSe_2$. *Nano Lett.* **2018**, *18*, 2311−2315.
(21) Liebhaber, E.; et al. Yu−shiba−rusinov states in the charge-density modulated superconductor $NbSe_2$. *Nano Lett.* **2020**, *20*, 339−344.
(22) Taniguchi, T.; Watanabe, K. Synthesis of high-purity boron nitride single crystals under high pressure by using ba−bn solvent. *Journal of crystal growth* **2007**, *303*, 525−529.
(23) Bardeen, J. Tunnelling from a many-particle point of view. *Physical review letters* **1961**, *6*, 57.
(24) Tersoff, J.; Hamann, D. R. Theory of the scanning tunneling microscope. *Phys. Rev. B* **1985**, *31*, 805.
(25) Dynes, R.; Narayanamurti, V.; Garno, J. P. Direct measurement of quasiparticle-lifetime broadening in a strong-coupled superconductor. *Phys. Rev. Lett.* **1978**, *41*, 1509.
(26) Foner, S.; McNiff, E., Jr Upper critical fields of layered superconducting $NbSe_2$ at low temperature. *Phys. Lett. A* **1973**, *45*, 429−430.
(27) Nader, A.; Monceau, P. Critical field of 2H-$NbSe_2$ down to 50mk. *SpringerPlus* **2014**, *3*, 16.
(28) Bauer, J.; Oguri, A.; Hewson, A. Spectral properties of locally correlated electrons in a bardeen−cooper−schrieffer superconductor. *J. Phys.: Condens. Matter* **2007**, *19*, 486211.
(29) Meng, T.; Florens, S.; Simon, P. Self-consistent description of andreev bound states in josephson quantum dot devices. *Phys. Rev. B* **2009**, *79*, 224521.
(30) Martín-Rodero, A.; Levy Yeyati, A. Josephson and andreev transport through quantum dots. *Adv. Phys.* **2011**, *60*, 899−958.
(31) Yu, L. Bound state in superconductors with paramagnetic impurities. *Acta Phys. Sin* **1965**, *21*, 75.
(32) Shiba, H. Classical spins in superconductors. *Progress of theoretical Physics* **1968**, *40*, 435−451.
(33) Rusinov, A. Superconductivity near a paramagnetic impurity. *JETP Lett.* **1969**, *9*, 146.
(34) Kezilebieke, S.; et al. Topological superconductivity in a van der waals heterostructure. *Nature* **2020**, *588*, 424−428.
(35) Chandni, U.; Watanabe, K.; Taniguchi, T.; Eisenstein, J. Evidence for defect-mediated tunneling in hexagonal boron nitride-based junctions. *Nano Lett.* **2015**, *15*, 7329−7333.
(36) Qiu, H.; et al. Hopping transport through defect-induced localized states in molybdenum disulphide. *Nat. Commun.* **2013**, *4*, 2642.
(37) Yu, Z.; et al. Towards intrinsic charge transport in monolayer molybdenum disulfide by defect and interface engineering. *Nat. Commun.* **2014**, *5*, 5290.
(38) Hong, J.; et al. Exploring atomic defects in molybdenum disulphide monolayers. *Nat. Commun.* **2015**, *6*, 6293.
(39) Vancsó, P.; et al. The intrinsic defect structure of exfoliated MoS_2 single layers revealed by scanning tunneling microscopy. *Sci. Rep.* **2016**, *6*, 29726.
(40) De Moor, M. W.; et al. Electric field tunable superconductor-semiconductor coupling in majorana nanowires. *New J. Phys.* **2018**, *20*, 103049.
(41) Fasth, C.; Fuhrer, A.; Samuelson, L.; Golovach, V. N.; Loss, D. Direct measurement of the spin-orbit interaction in a two-electron inas nanowire quantum dot. *Physical review letters* **2007**, *98*, 266801.
(42) O'Farrell, E.; et al. Hybridization of subgap states in one-dimensional superconductor-semiconductor coulomb islands. *Physical review letters* **2018**, *121*, 256803.

https://doi.org/10.1021/acs.nanolett.2c02777
Nano Lett. 2023, 23, 2454−2459